MECHANISMS FOR THE RIGID ROTATION OF CORONAL HOLES

A. G. NASH, N. R. SHEELEY, JR., and Y.-M. WANG*

E.O. Hulburt Center for Space Research, Naval Research Laboratory, Washington, D.C. 20375–5000, U.S.A.

(Received 15 February, 1988; in revised form 22 April, 1988)

Abstract. We show that the rotation of coronal holes can be understood in terms of a current-free model of the coronal magnetic field, in which holes are the footpoint locations of open field lines. The coronal field is determined as a function of time by matching its radial component to the photospheric flux distribution, whose evolution is simulated including differential rotation, supergranular diffusion, and meridional flow. We find that ongoing field-line reconnection allows the holes to rotate quasi-rigidly with their outer-coronal extensions, until their boundaries become constrained by the neutral line of the photospheric field as it winds up to form stripes of alternating magnetic polarity. This wind-up may be significantly retarded by a strong axisymmetric field component which forces the neutral line to low latitudes; it is also gradually halted by the cross-latitudinal transport of flux via supergranular diffusion and a poleward bulk flow. We conclude that a strong axisymmetric field component is responsible for the prolonged rigid rotation of large meridional holes during the declining phase of the sunspot cycle, but that diffusion and flow determine the less rigid rotation observed near sunspot maximum, when the holes corotate with their confining polarity stripes.

1. Introduction

This paper examines the mechanisms for the quasi-rigid rotation of holes in the Sun's lower corona. Such coronal holes have been observed routinely in X-ray, XUV, and He I 10830 Å images, and are believed to represent the footpoint locations of open magnetic field lines (see the reviews of Axford, 1977; Zirker, 1977a, b; Harvey and Sheeley, 1979; Wilson, 1979). During the declining phase of sunspot cycle 20, coronal holes rotated almost as rigidly as white-light features in the outer corona (Timothy, Krieger, and Vaiana, 1975; Wagner, 1975; Bohlin, 1977), and maintained quasi-vertical shapes as exemplified by the well-known Skylab Coronal Hole 1 (CH1). On the other hand, during the rising and maximum phases of sunspot cycle 21, holes rotated less rigidly and were often skewed in the direction of the photospheric differential rotation (Sheeley and Harvey, 1978, 1981; Shelke and Pande, 1985; Harvey and Sheeley, 1987).

Coronal holes are observed to lie within the boundaries of unipolar magnetic regions on the photosphere (McIntosh *et al.*, 1976; Bohlin and Sheeley, 1978), which in turn have long been known to rotate more rigidly than the photospheric plasma itself (Bumba and Howard, 1965; Wilcox and Howard, 1970; Wilcox *et al.*, 1970; Schatten *et al.*, 1972; Stenflo, 1974, 1977). Consequently, when we recently discovered a mechanism which naturally accounts for these rigidly-rotating patterns, we suggested that it might also explain the rigid behavior of coronal holes (Sheeley, Nash, and Wang, 1987, hereafter Paper I). The mechanism involves the effect of supergranular diffusion,

* Applied Research Corporation, Landover, MD 20785, U.S.A.

Solar Physics **117** (1988) 359–389.

possibly accompanied by a small poleward flow; these processes transport magnetic flux across latitudes and thus gradually offset the shearing effect of differential rotation on the magnetic polarity patterns.

The latitudinal flux-transport mechanism provides a satisfactory explanation for the rotation rates exhibited by coronal holes near sunspot maximum, as they become confined within striped patterns of alternating magnetic polarity. However, it seems unable to account for the large, relatively undistorted holes seen near sunspot minimum, such as Skylab CH1, which extended from the north pole into the southern hemisphere and maintained its vertical shape for seven rotations (Timothy, Krieger, and Vaiana, 1975). At their leisurely rates, diffusion and flow would require several months before they could cause a large structure like CH1 to rotate rigidly; moreover, the rigid rotation that eventually results would occur at a different rate near the equator than near the poles (see Appendix C of Paper I). Thus, for a coronal hole to remain relatively undistorted from the time of its formation, the rotation must apparently be closely tied to that of the outer corona, which always rotates more rigidly than the photospheric field (Hansen, Hansen, and Loomis, 1969; Parker, Hansen, and Hansen, 1982; Fisher and Sime, 1984; Parker, 1986).

In this investigation, we use a current-free extension of the photospheric field to determine the rotational properties of coronal holes. Those field lines which extend out to a spherical 'source surface' are considered to be open, and their photospheric footpoints are taken to define the coronal-hole areas. Hoeksema (1984) and Hoeksema and Scherrer (1987) have shown that the magnetic field at the source surface exhibits quasi-rigid rotation similar to that observed in the outer white-light corona. Recently, we demonstrated that this rigid behavior is a natural consequence of the increasing dominance of low-order multipoles of the magnetic field with height (Wang *et al.*, 1988, hereafter Paper II). In the present paper, we show that coronal holes nearly corotate with their source-surface extensions until they become confined between stripes of the photospheric polarity pattern. This allows us to understand the differences between the rotation of coronal holes near sunspot maximum and minimum in terms of the role of the Sun's axisymmetric field component in hindering the formation of stripes.

The organization of this paper is as follows. Section 2 describes our procedure for modelling coronal holes. In Section 3, we present numerical simulations of coronal-hole rotation for various initial field configurations. The Appendix contains supporting analytical calculations that describe the wind-up of a tilted-dipole field. Finally, we summarize and discuss our results in Section 4.

2. The Model

The physical assumption underlying our study of coronal-hole rotation is that the corona may be considered approximately current-free, so that the large-scale coronal field satisfies $\nabla \times \mathbf{B} = 0$ at all times during its evolution. In particular we apply the source-surface technique of Schatten, Wilcox, and Ness (1969) and Altschuler and Newkirk (1969), which has been frequently used to model large-scale magnetic features in the

corona (for references, see Hoeksema, 1984). The procedure is to solve Laplace's equation within the spherical cavity $R_\odot < r < R_s$, subject to the conditions that the nonradial components of the field vanish at the 'source source' $r = R_s$ and that the radial component of the field match the given photospheric distribution at $r = R_\odot$. (The model implicitly assumes the presence of electrical currents in the region $r \geq R_s$. For purposes of the present paper, the 'corona' will be identified with the current-free region within the source surface.) We define 'open' field lines to be those that reach the source surface; their photospheric footpoints will be taken to represent 'coronal hole' areas (cf. Levine *et al.*, 1977; Pneuman, Hansen, and Hansen, 1978).

We assume that the time evolution of the radial component of the photospheric field, which represents the inner boundary condition of the system, can be described by the flux-transport equation

$$\frac{\partial B_{ph}}{\partial t} = -\omega(\theta)\frac{\partial B_{ph}}{\partial \phi} - \frac{1}{R_\odot \sin\theta}\frac{\partial}{\partial \theta}\left[B_{ph} v(\theta)\sin\theta\right] + \\ + \frac{\kappa}{R_\odot^2}\left[\frac{1}{\sin\theta}\frac{\partial}{\partial\theta}\left(\sin\theta\frac{\partial B_{ph}}{\partial\theta}\right) + \frac{1}{\sin^2\theta}\frac{\partial^2 B_{ph}}{\partial\phi^2}\right] + S\,. \tag{1}$$

(For a discussion of the derivation of this equation, see DeVore, Sheeley, and Boris, 1984). Here θ is the colatitude angle, ϕ the longitude angle, and t the elapsed time; $\omega(\theta)$ represents the intrinsic rate of differential rotation of the photospheric field, $v(\theta)$ is the meridional flow velocity due to laminar bulk motion, and κ denotes the rate at which magnetic flux is effectively diffused by supergranular convective motions. Ongoing eruptions of flux on the photosphere are represented by the source term S. In this paper, we consider for the most part idealized cases for which $S = 0$, involving the evolution of a given configuration of photospheric flux. It should be noted, however, that since new sources may contribute open as well as closed magnetic flux, they can rapidly affect the shape and distribution of coronal-hole areas.

For a given initial photospheric flux distribution, we solve Equation (1) using the numerical code described by Sheeley, DeVore, and Boris (1985). Knowing $B_{ph}(\theta, \phi, t)$, we then determine the coefficients $a_{lm}(t)$ of its expansion in terms of spherical harmonics:

$$B_{ph}(\theta, \phi, t) = \sum_{l=1}^{\infty}\sum_{m=-l}^{l} a_{lm}(t)\, Y_{lm}(\theta, \phi)\,. \tag{2}$$

Requiring that the radial component $B_r(r, \theta, \phi, t)$ of the potential-field solution reduce to $B_{ph}(\theta, \phi, t)$ at $r = R_\odot$ and that the tangential components $B_\theta(r, \theta, \phi, t)$ and $B_\phi(r, \theta, \phi, t)$ vanish at $r = R_s$, we then obtain the three components of the coronal field:

$$B_r(r, \theta, \phi, t) = \sum_{lm} a_{lm}(t)\, c_l(r)\, Y_{lm}(\theta, \phi)\,, \tag{3a}$$

$$B_\theta(r, \theta, \phi, t) = -\sum_{lm} a_{lm}(t)\, d_l(r)\frac{\partial Y_{lm}(\theta, \phi)}{\partial\theta}\,, \tag{3b}$$

$$B_\phi(r, \theta, \phi, t) = -\sum_{lm} im\, a_{lm}(t) d_l(r) \frac{Y_{lm}(\theta, \phi)}{\sin\theta} . \tag{3c}$$

Here the coefficients $c_l(r)$ and $d_l(r)$ are given by

$$c_l(r) = \left(\frac{R_\odot}{r}\right)^{l+2} \left[\frac{l + 1 + l(r/R_s)^{2l+1}}{l + 1 + l(R_\odot/R_s)^{2l+1}}\right], \tag{4a}$$

$$d_l(r) = \left(\frac{R_\odot}{r}\right)^{l+2} \left[\frac{1 - (r/R_s)^{2l+1}}{l + 1 + l(R_\odot/R_s)^{2l+1}}\right]. \tag{4b}$$

From Equations (4), it may be seen that $c_l(R_\odot) = 1$ and $d_l(R_s) = 0$, so that the boundary conditions $B_r = B_{ph}$ at $r = R_\odot$ and $B_\theta = B_\phi = 0$ at $r = R_s$ are indeed satisfied. (We remark that the field lines need not be radial at the source surface along neutral lines where B_r vanishes.) On the other hand, since $d_l(R_\odot) \neq 0$, the potential-field model requires the presence of nonradial components of the field at the photosphere. In Equation (1), however, the diffusion terms proportional to κ were derived by neglecting tangential components of the photospheric field. The assumption that the large-scale photospheric field is predominantly radial is supported by magnetograph observations (see, e.g., Howard and LaBonte, 1981). This apparent inconsistency can be resolved by postulating the existence of strong currents within a narrow 'boundary layer' just above the photosphere, which generate the nonradial components required to match the potential-field solution. In the framework of the present model, the boundary layer may be idealized as a current sheet located at $r = R_\odot$, across which B_r is continuous but the tangential components of the field change discontinuously. There is observational evidence, from magnetograms in spectral lines originating in the chromosphere, for a rapid deflection of field lines above the photosphere to form 'canopy' structures (see, e.g., Chapman and Sheeley, 1968; Pope and Mosher, 1975; Giovanelli, 1980; Jones, 1985); also, horizontal magnetic fields have been inferred indirectly from Hα pictures of chromospheric fibril structure (Veeder and Zirin, 1970). Such observations have been interpreted by many authors (e.g., Giovanelli, 1980) as indicating the presence of chromospheric currents and locally non-potential fields, although current-free models have also been suggested (e.g., Gabriel, 1976).

Having determined the coronal field, we locate coronal holes by numerically tracing field lines from the source surface down to the photosphere. By cross-correlating the footpoint areas at intervals of approximately 27 days, we finally obtain the rotation profiles of the simulated holes.

In practice, we employed a grid of 128 cells equally spaced in longitude and 64 cells equally spaced in latitude to compute the photospheric field B_{ph}, and truncated the spherical-harmonic expansions (3) above $l = 25$. We traced 128 × 64 field lines, uniformly spaced at $r = R_s$, down to $r = R_\odot$ by evaluating the coronal field at intervals of $\Delta r = 0.01\, R_\odot$. Unless otherwise noted, the source surface was arbitrarily placed at $R_s = 2.0\, R_\odot$. The cross-correlations were performed on individual holes (rather than on

the entire footpoint maps), and were based on the hole boundaries, not on the field-strength distribution within them. As will become apparent below, a composite rotation profile encompassing more than one hole may have little meaning because the rotational properties of individual holes vary widely.

Before proceeding to describe the individual simulations in detail, we summarize briefly the main physical constraints to which our model subjects the evolution of a coronal hole. First, the holes must (by definition) remain connected by field lines to the source surface. Second, the field lines must continually adjust their topology so as to ensure that the coronal field remains curl-free at all times. Third, the hole boundaries must remain within unipolar photospheric regions of the proper polarity.

3. Simulation Results

We now present our numerical simulations of the evolution of coronal holes, organizing the results according to the initial distribution of photospheric flux that we assume.

3.1. Initial horizontal dipole field

We start by examining the behavior of a horizontal dipole configuration, for which the dipole and rotation axes are mutually perpendicular and no axisymmetric component of the field is present. Figure 1(a) shows the evolution of the associated coronal holes when the only flux-transport mechanism present on the photosphere is differential rotation with the Newton and Nunn (1951) profile $\omega(\theta) = \omega_0 - \omega_1 \cos^2 \theta$. The holes are shown superimposed on the photospheric polarity distribution (left column) and on the polarity distribution of the source-surface field (right column). The time intervals between the instantaneous maps are multiples of the 26.9-day equatorial rotation period of the photosphere.

As the initial equatorial holes (one of each polarity) start to deform, they move eastward in the 26.9-day equatorial system, but then come to rest 45° from their initial positions after about one wind-up time ($2\pi/\omega_1 = 4.8$ rotations). With each subsequent wind-up of the photospheric flux distribution, a narrow 'auxiliary' hole appears at higher latitudes within each newly-formed polarity stripe. These new holes in turn successively drift eastward until they come into longitudinal coalignment with their predecessors of like polarity. Thus, the holes form two growing stacks which are stationary in the equatorial system and rotate in phase with the corresponding polarity patterns of the source-surface field, as shown in the right column of Figure 1(a).

On the other hand, the confining photospheric polarity stripes continue to rotate differentially at the rate $\omega(\theta)$. In order to remain stationary in the equatorial system, the longitudinally-coaligned holes migrate equatorward along the slanted stripes. As Figure 1(b) indicates, the coronal-hole boundaries (measured at a fixed latitude) rotate at nearly the local differential rate $\omega(\theta)$ after about a wind-up time (4.8 rotations).

As long as the photospheric flux distribution continues to wind-up, the hole boundaries will rotate differentially and the hole centers will drift toward the equator. As demonstrated in Paper I, however, the transport of flux across latitudes by super-

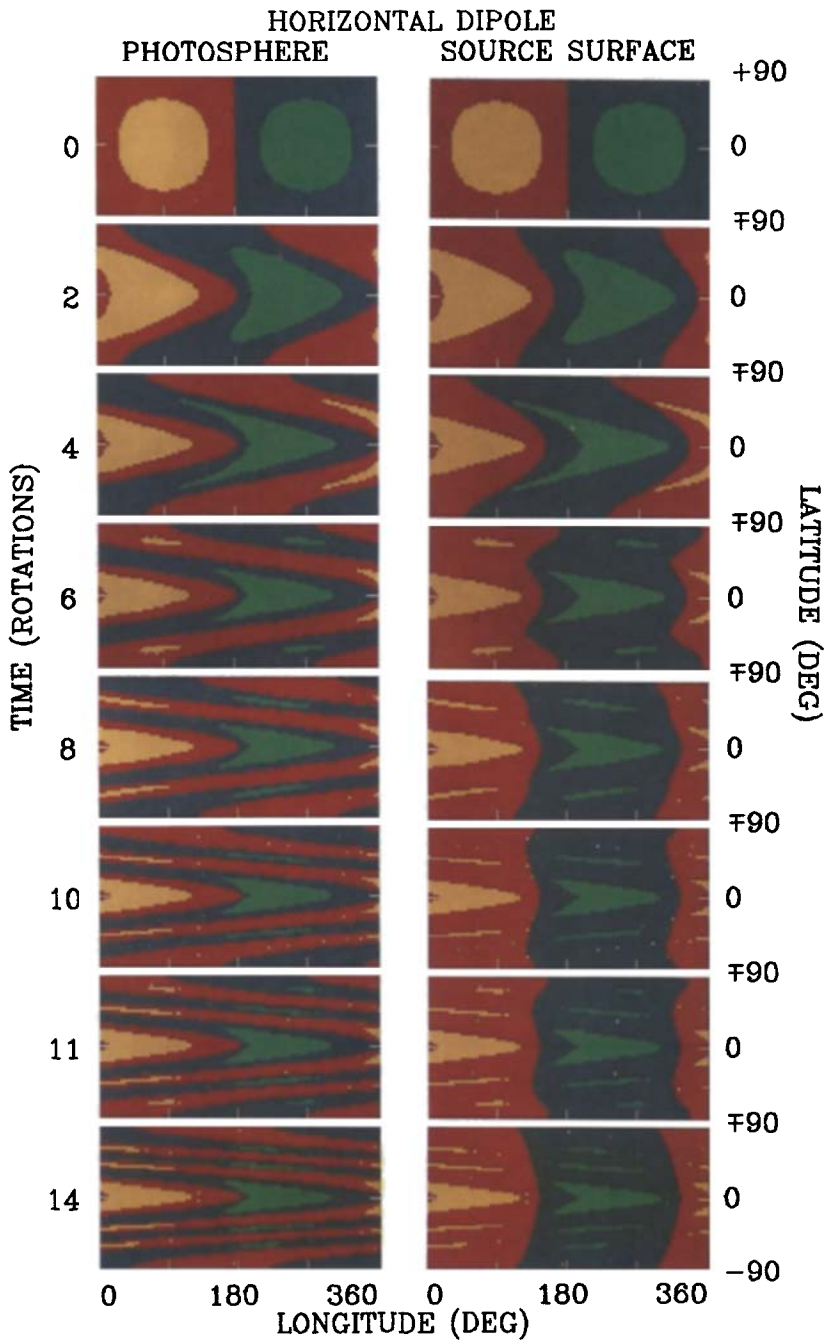

Fig. 1a. Evolution of an initial horizontal-dipole configuration in the presence of differential rotation alone. The maps show the instantaneous polarity patterns of the photospheric field (left column) and of the source-surface field at 2.0 $R_\odot$ (right column), with red and blue used to denote opposite polarities of the radial field. The footpoint locations of open field lines (coronal holes) corresponding to the red and blue polarities are indicated by the yellow and green areas, respectively.

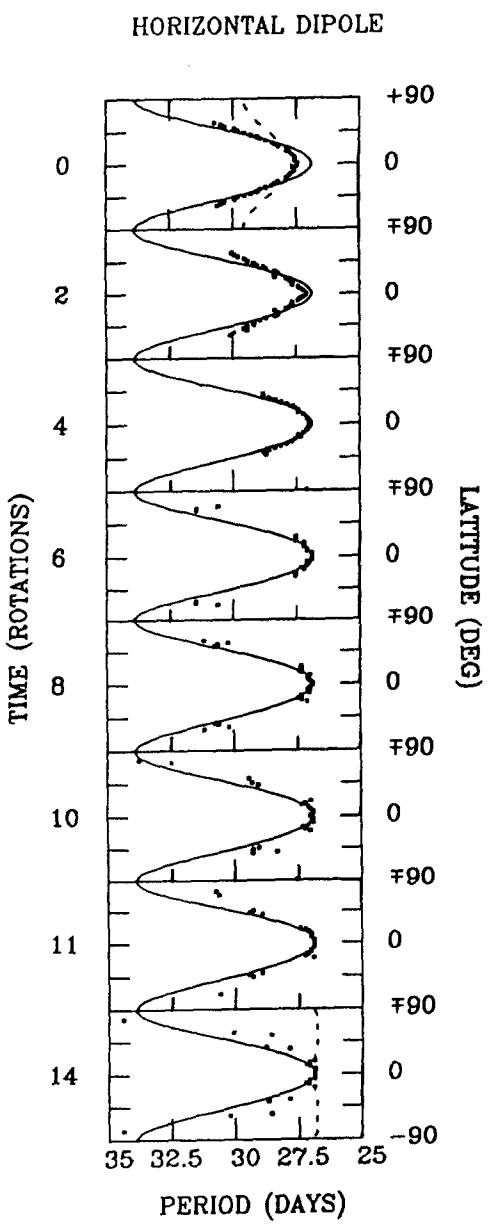

Fig. 1b. Rotation profiles for the coronal holes of either polarity in Figure 1(a) are indicated by large dots. For comparison, we also show the Newton–Nunn rotation curve obeyed by the photospheric field (solid lines), and the rotation profiles of the source-surface field projected onto its photospheric footpoints (dashed lines in the first and last frames).

granular diffusion or meridional flow will act to offset the shearing of the polarity patterns, eventually preventing the formation of new stripes and causing those already present to rotate rigidly. We therefore expect the inclusion of diffusion or meridional

flow to lead to the eventual rigid rotation of the hole boundaries which are embedded within the stripes.

The left column of Figure 2(a) illustrates how the holes evolve when the Newton–Nunn differential rotation is accompanied by diffusion at a nominal 600 $km^2 s^{-1}$ rate, for the same initial horizontal-dipole configuration. During the first wind-up time, the diffusion has essentially no effect since the spatial gradients of the flux distribution are still small. However, after about 10 rotations, no further stripes are produced and only the equatorial holes survive. At this point, the equatorward motion ceases and the holes rotate rigidly with the source-surface field. One can also see that diffusion not only counteracts the shearing of the photospheric flux distribution, but suppresses smaller-scale structures including the sharp edges of the equatorial holes as well as the 'auxiliary' holes themselves. As shown by the corresponding rotation profiles in the left column of Figure 2(b), the remnant equatorial holes rotate rigidly with the 27.0-day period that characterizes the asymptotic rotation of the decaying polarity stripes at lower latitudes (see Paper I; DeVore, 1987). This slight difference from the 26.9-day equatorial period gives rise to the slow, continual eastward drift of the holes which may be discerned in Figure 2(a). Finally, it is interesting to note that since the photospheric polarity pattern above latitude 45° attains a different asymptotic state of rotation close to the polar rate, the high- and low-latitude stripes in Figure 2(a) rotate periodically past one another.

The right column of Figure 2(a) illustrates the behavior when diffusion is replaced by a poleward bulk flow of the form $v(\theta) = -v_0 \sin(2\theta)$. The peak flow speed v_0 has been assigned a nominal value of 20 m s^{-1}, consistent with the observations of Duvall (1979). Again, the latitudinal transport of flux has little noticeable effect during the first wind-up time, but gradually an equilibrium is established between the shearing and the poleward flow which prevents further stripes from forming at lower latitudes (new stripes become crowded toward the poles). As shown in the right column of Figure 2(b), the rotation profiles of both the coronal holes and the photospheric polarity patterns then become increasingly rigid at the 26.9-day equatorial period as time passes, starting near the equator and progressing to higher latitudes.

In all three of the above examples, the coronal holes initially rotate more rigidly than the photospheric field, but less rigidly than the source-surface field. The physical mechanism that frees the holes from the motion of the photospheric flux elements is the reconnection of field lines at the hole boundaries. Reconnection opposes the shearing of the footpoint areas and ensures that the coronal field remains curl-free. Its effect is illustrated by Figure 3, which compares the shapes of the coronal holes in Figure 1(a) with the shapes that they would have had if they had rotated differentially with the photospheric flux from one frame to the next. As expected, the difference is greatest during the first wind-up time, before the holes become narrowly confined by stripes. After 7 rotations, the field-line reconnection occurs principally at the leading and trailing ends of the holes, allowing them to remain in phase with the rigidly-rotating source-surface field as they drift equatorward within their confining polarity stripes.

As shown in the Appendix, field-line reconnection occurs in three stages during the

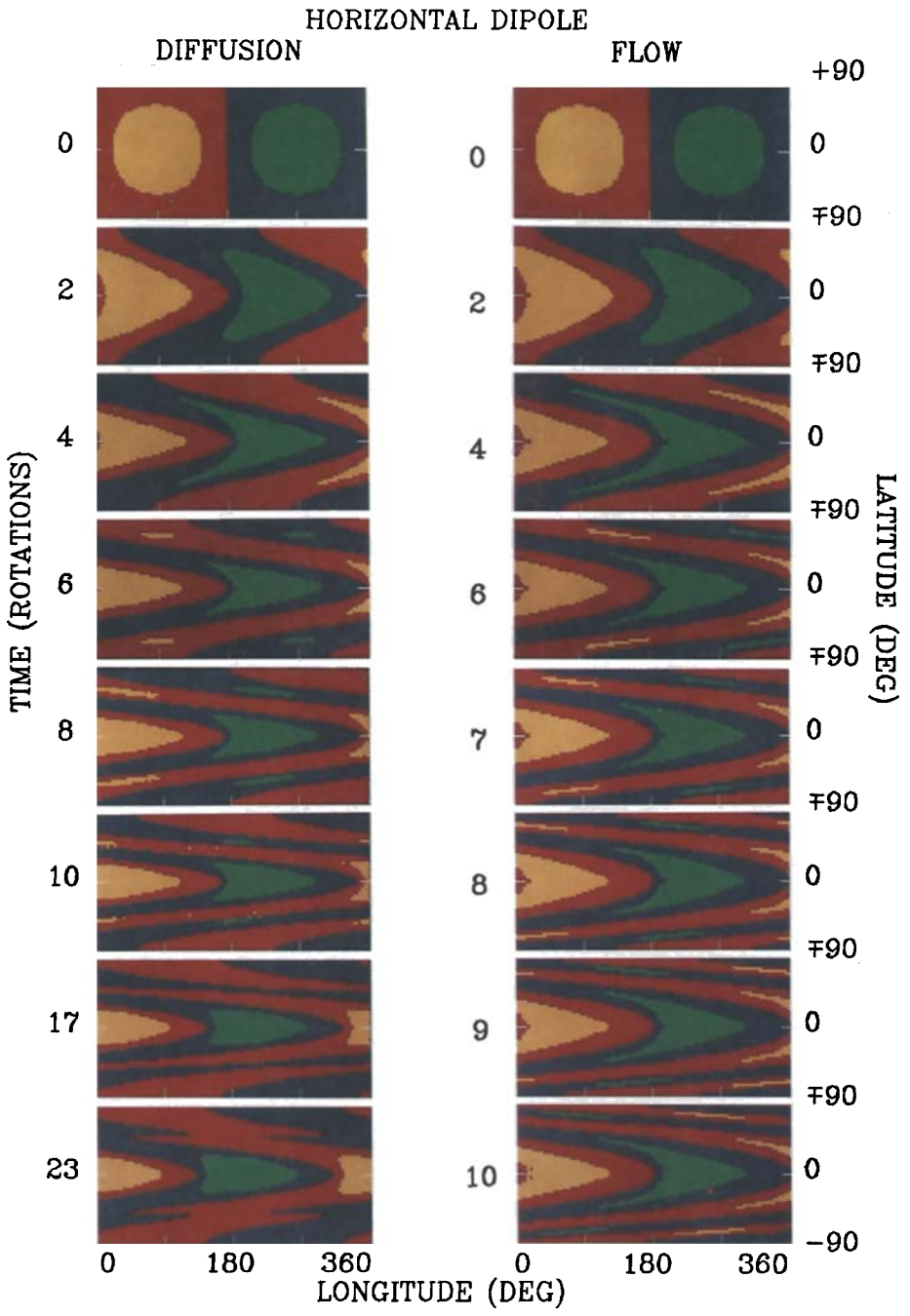

Fig. 2a. Evolution of an initial horizontal-dipole configuration when differential rotation is accompanied by supergranular diffusion at a 600 $km^2\ s^{-1}$ rate (left column), and when differential rotation is accompanied by a poleward flow with a peak speed of 20 $m\ s^{-1}$ (right column). The maps show the instantaneous polarity patterns of the photospheric field, with coronal holes indicated by the yellow and green areas superimposed on the corresponding red- and blue-polarity regions.

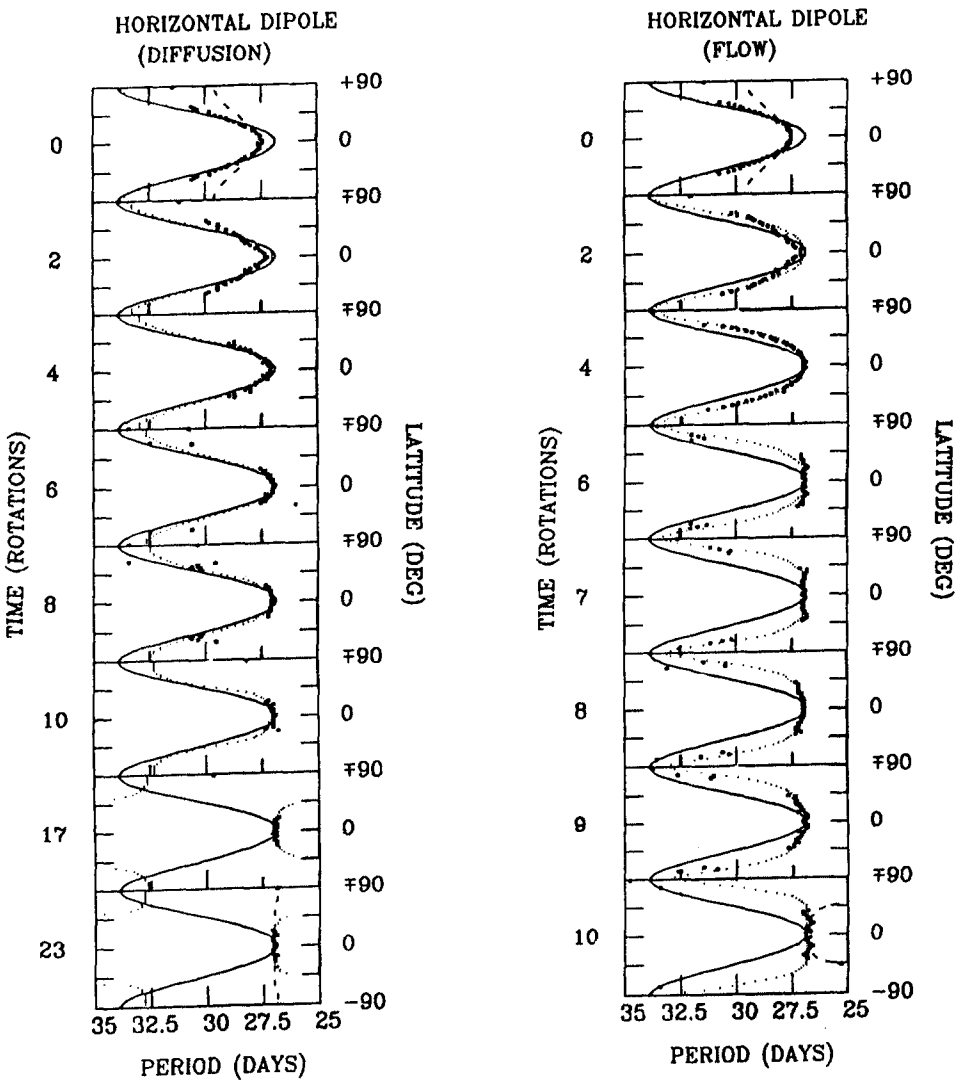

Fig. 2b. Rotation profiles for the coronal holes of either polarity corresponding to the two cases shown in Figure 2(a) are indicated by the large dots. For comparison, we also display the Newton–Nunn rotation curve (solid lines), the projected rotation profile of the source-surface field (dashed lines in the first and last frames), and the rotation profiles of the photospheric polarity patterns (dotted lines).

evolution of the horizontal-dipole configuration. During the initial stage ($t \ll \tau_w$), the total amount of open flux threading the source surface is conserved, and the open field lines simply change their footpoint connections in such a way as to oppose the photospheric shearing. These field-line rearrangements occur below the source surface, despite the fact that no neutral points have yet formed there. During the intermediate stage ($t \sim \tau_w$), the amount of open flux decreases rapidly to about 50% of its initial value as differential rotation continues to stretch the photospheric neutral line. This recon-

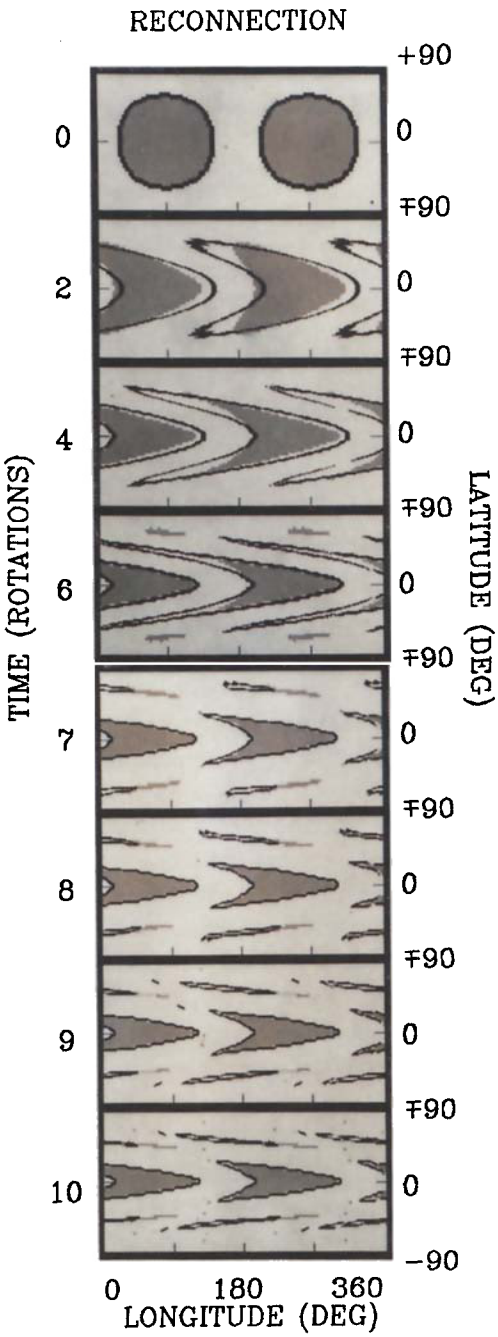

Fig. 3. The evolution of the coronal holes in Figure 1(a) (indicated by the gray areas) is compared with the distortion that their boundaries would have undergone (indicated by the solid black lines) if they had moved with the photospheric flux since the time of the preceding frame. Magnetic field-line reconnection must occur where differences are seen.

nection takes place at the source-surface neutral line, where open field lines merge and are converted into closed flux. During the final stage ($t > \tau_w$), the open flux decays relatively slowly, eventually as $t^{-1/2}$. Reconnection now occurs not only at the source-surface neutral line, where open flux continues to be closed down, but also at neutral lines formed in the lower corona with each succeeding wind-up, where a portion of the

open flux is transferred from the equatorial coronal holes to the auxiliary holes at higher latitudes.

3.2. Initial tilted-dipole field: effect of the axisymmetric component

We may gain further insight into the rotation of coronal holes by adding an axisymmetric component to the photospheric flux distribution. For simplicity, we consider the wind-up of a tilted-dipole configuration, which represents the superposition of a horizontal and a vertical dipole field. Figure 4(a) illustrates the evolution of the coronal holes when the dipole axis is inclined by 60° relative to the rotation axis and only differential rotation is present. This simulation shows several of the features of the horizontal-dipole case discussed above, including the initial deformation and 45° eastward drift of the large axial holes, their co-alignment with the corresponding polarity patterns of the source-surface field, and the build-up of stacks of auxiliary holes which rotate with the source-surface field at the 26.9-day equatorial rate. Again, even though the stacks remain stationary in the equatorial system, the hole boundaries rotate differentially (Figure 4(b)) and the individual holes themselves migrate equatorward.

However, the evolution of the tilted-dipole configuration contains some unique features not present in the horizontal-dipole case. First, during the initial wind-up time, the original holes rapidly spread poleward to form eccentric polar holes. This behavior is due to the symmetrization of the coronal field by differential rotation, which acts to reduce the contribution of the nonaxisymmetric components by converting them into high-order multipoles (see Appendix, Part C). Second, as wind-up proceeds, new holes are produced by shearing off increasingly high-latitude segments of the polar-hole 'lobes'. Thus a hole is formed each time a stripe of opposite-polarity flux encroaches into a polar-hole lobe. Clearly, this would not occur if the lobes were initially located above the photospheric neutral line at every longitude, as could be achieved by decreasing the dipole tilt angle and thus strengthening the axisymmetric component of the field. Third, since the nonaxisymmetric components of the source-surface field vanish in the limit $t \to \infty$, the auxiliary holes must eventually disappear, leaving only the two axisymmetric polar holes which represent the vertical-dipole component of the field.

Finally, we note that there is an appreciable difference between the initial rotation of the tilted-dipole and horizontal-dipole coronal holes (compare Figures 1(b) and 4(b)). At latitudes above about 30°, the tilted-dipole hole shows a much faster and more rigid rotation rate than the photospheric field, which is not the case for the horizontal-dipole hole at high latitudes. In attempting to understand this behavior, we have considered the possibility that the coronal-hole boundaries in both cases initially corotate with their source-surface extensions. Thus we have also plotted in the initial frames of Figures 1(b) and 2(b) and Figures 4(b), 5(b), and 6(b) the profiles obtained by projecting the rotation rate of the source-surface neutral lines onto the photosphere along the connecting field lines, as described by equation (A6) of the Appendix. These profiles may be seen to provide a crude zeroth-order approximation to the actual coronal-hole rotation curves (although the agreement becomes very poor at high latitudes), suggesting that the more rigid rotation of the tilted-dipole hole is related to the mapping of its boundaries to lower

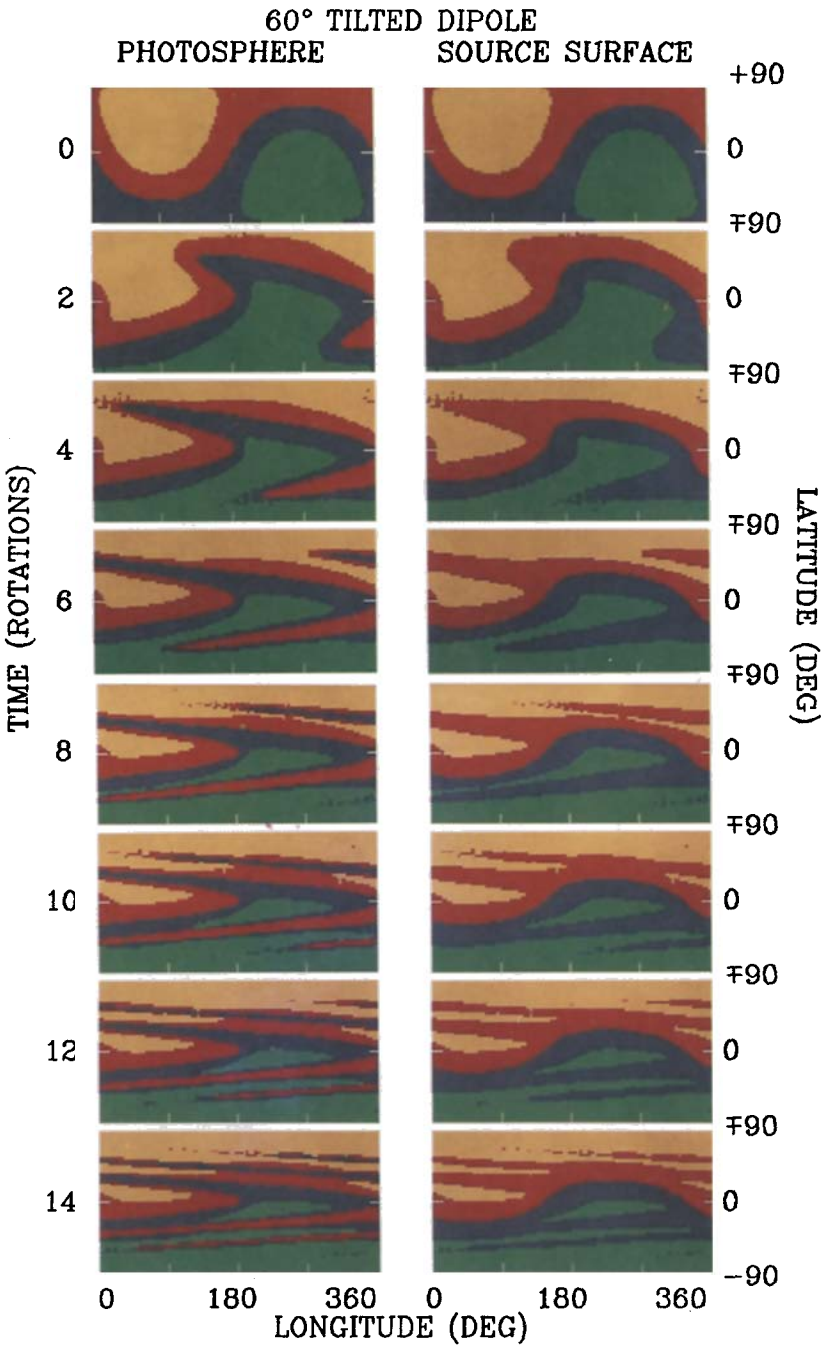

Fig. 4a. Evolution of an initial 60° tilted-dipole configuration in the presence of differential rotation alone. The maps show the instantaneous polarity patterns of the photospheric field (left column) and of the source-surface field at 2.0 $R_{\odot}$ (right column). As in previous figures, coronal holes are indicated by the yellow and green areas corresponding to red and blue polarities of the radial field.

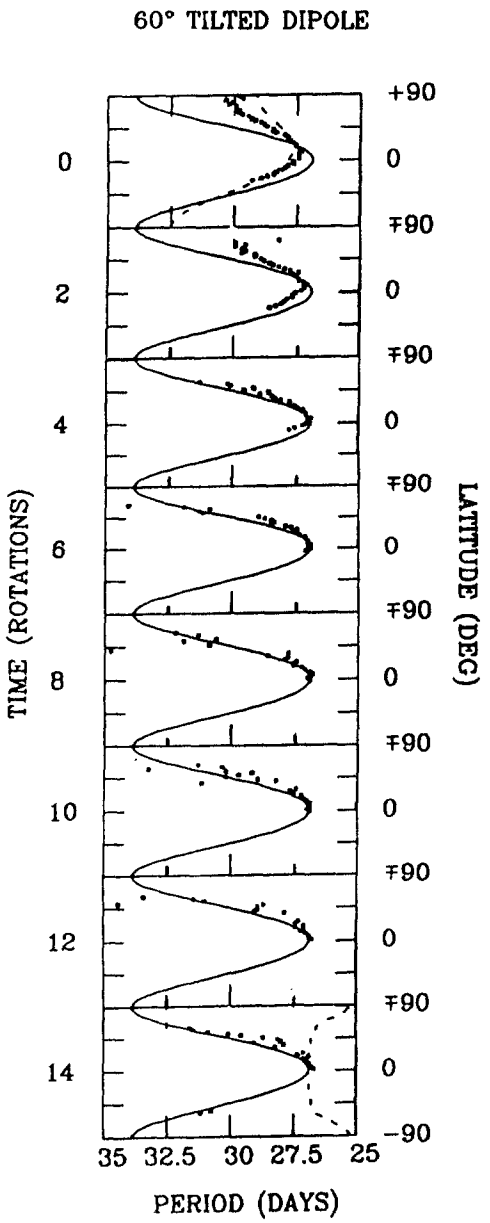

Fig. 4b. Rotation profiles for the yellow coronal holes of Figure 4(a) are indicated by the large dots. Again shown for comparison are the Newton–Nunn rotation curve obeyed by the photospheric field (solid lines) and the projected rotation profile of the source-surface field (dashed lines in the first and last frames).

latitudes at the source surface. In fact we do not expect exact corotation between the holes and their source-surface extensions because the rotation rate of the hole boundary represents a global average involving the rotation rates of all three components of the coronal field at all intermediate heights (as described in part B of the Appendix). As

mentioned above, the large deviations of the initial coronal-hole rotation profiles from the photospheric rate $\omega(\theta)$ requires the ongoing reconnection of field lines at the hole boundaries.

Figures 5(a) and 5(b) show the effect of decreasing the tilt angle of the dipole field to 45°. Here, we have also reduced the half-angle of the initial axial holes from 57.2° to 22° by moving the source surface from $R_s = 2\,R_\odot$ to $R_s = 10\,R_\odot$. The small size of the holes makes their poleward and eastward migration during the first wind-up time particularly striking. Because the photospheric neutral line is confined to latitudes below 45°, each polar-hole lobe is now severed only once by the intrusion of an opposite-polarity stripe. As the profiles of Figure 5(b) indicate, the rotation periods of the polar lobes subsequently oscillate around the 26.9-day equatorial value. Again, it is the continual reconnection of field lines that allows these high-latitude holes to rotate at approximately the equatorial rate while the ambient photospheric flux rotates at the local, much slower differential rate $\omega(\theta)$.

In the simulation of Figure 6(a), we have added diffusion at a rate $\kappa = 600\ \mathrm{km^2\ s^{-1}}$ to the 60° tilted-dipole configuration of Figure 4(a). The ability of diffusion to prevent stripes from shearing off new holes becomes apparent after 1–2 wind-up times (approximately 5–10 rotations). Eventually there remain only the large eccentric polar holes, whose lobes are again co-aligned with the source-surface polarity patterns. The profiles of Figure 6(b) show that after about 12 rotations, these holes rotate rigidly at the near-equatorial period of 27.0 days in a latitude band extending from the equator to above 45°. By contrast, the photospheric field patterns above 45° asymptotically rotate at a quasi-polar period of 32.8 days (Paper I; DeVore, 1987). As in the previous example, the ability of the holes to follow the source-surface field at these latitudes can be attributed to ongoing field-line reconnection. After a very long time, of course, the nonaxisymmetric components of the source-surface field will have decayed away and the holes must become purely axisymmetric and centered around the poles.

3.3. Simulation of Coronal Hole 1

As a final example, we show in Figure 7(a) the evolution of a coronal hole similar to Skylab's Coronal Hole 1 (Timothy, Krieger, and Vaiana, 1975). We generated this hole by depositing onto our photospheric grid five magnetic doublets having approximately the same strengths, locations, and eruption times as those observed on magnetograms a few months before the formation of CH1. The polar field was represented by a nominal 1G vertical dipole. We then let this flux evolve according to Equation (1), using the empirical formula of Snodgrass (1983) for the differential rotation rate, and including supergranular diffusion at a rate of $600\ \mathrm{km^2\ s^{-1}}$ and a latitude-independent poleward flow of magnitude $10\ \mathrm{m\ s^{-1}}$. To facilitate comparison with observations, the instantaneous maps are displayed at intervals of the 27.275-day Carrington period, rather than the 26.9-day equatorial period used in the preceding figures.

In the second panel of Figure 7(a), the positive-polarity hole resembles CH1 as observed in May 1973 at the beginning of the Skylab mission. Again like CH1, the simulated coronal hole retains its quasi-vertical shape until it decays 6–7 rotations later.

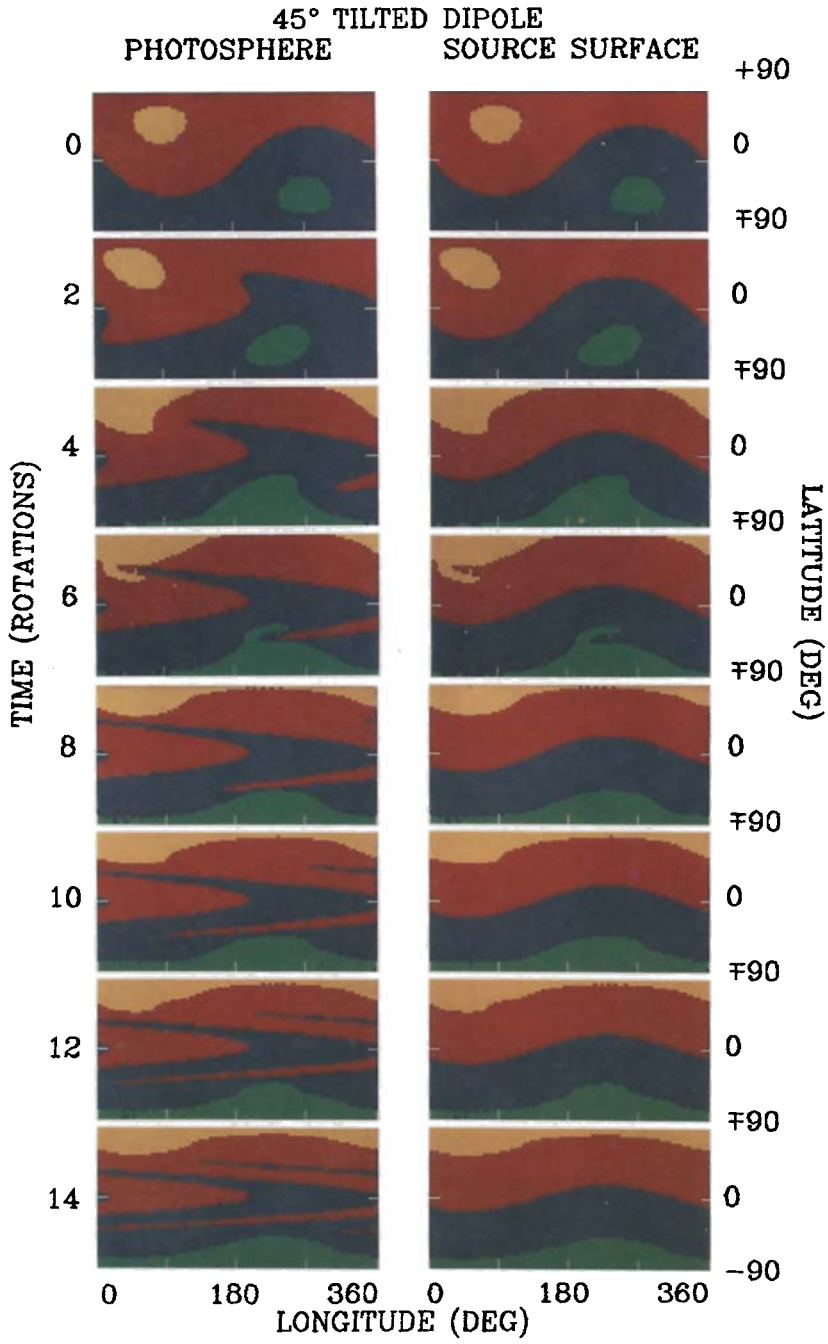

Fig. 5a. Same as Figure 4(a), except that the dipole tilt-angle has been reduced to 45° and the source surface has been moved out to 10 $R_{\odot}$. The small eccentric polar holes are now cut only once by the relatively low-latitude neutral line of the photospheric field.

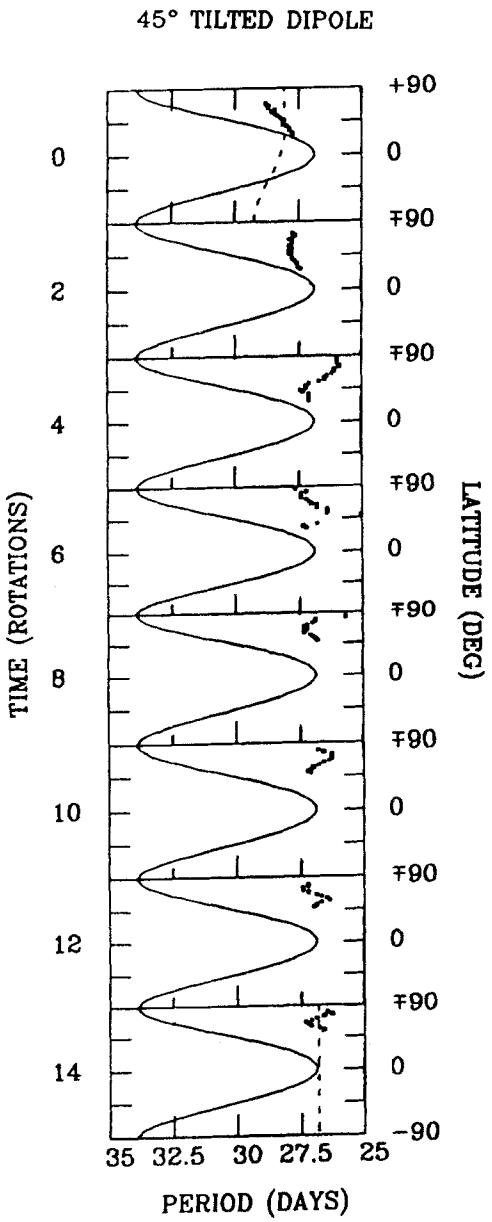

Fig. 5b. Rotation profiles for the yellow coronal hole of Figure 5(a) in the same format as Figure 4(b). After about one wind-up time (4.8 rotations), the rotation period of this high-latitude hole begins to oscillate around the 26.9-day equatorial value.

We emphasize that it is the axisymmetric component of the field which is principally responsible for prolonging the rigid rotation of the hole, by forcing the neutral line to lower latitudes where the wind-up rate $\omega'(\theta)$ is relatively small. This retards the intrusion of opposite-polarity stripes into the polar-hole lobe. The corresponding

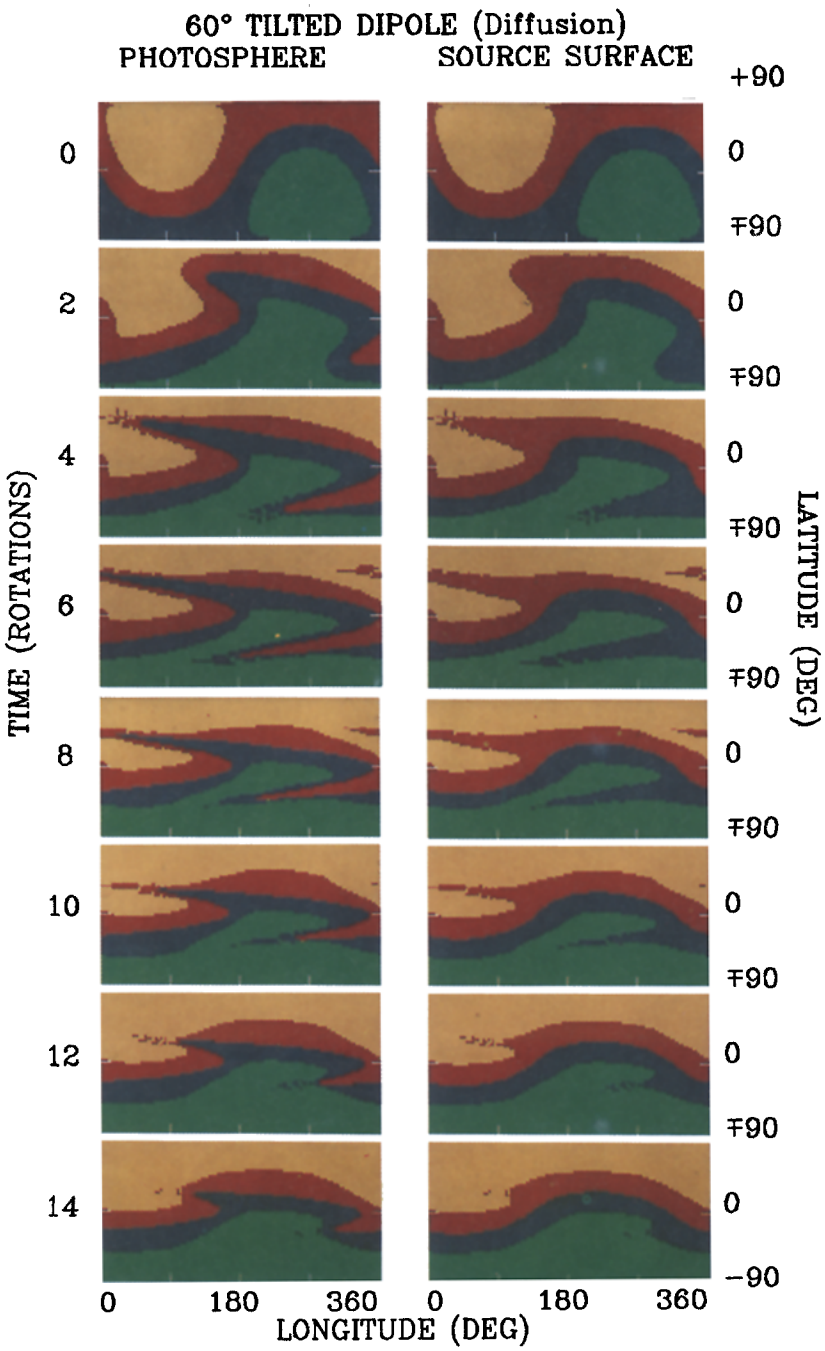

Fig. 6a. As in Figure 4(a), the initial configuration is a 60° tilted-dipole field, but the photospheric differential rotation is now accompanied by supergranular diffusion at a 600 $km^2 s^{-1}$ rate. The stripes disappear after 2–3 wind-up times (10–14 rotations), and the hole boundaries become contoured along the source-surface neutral line.

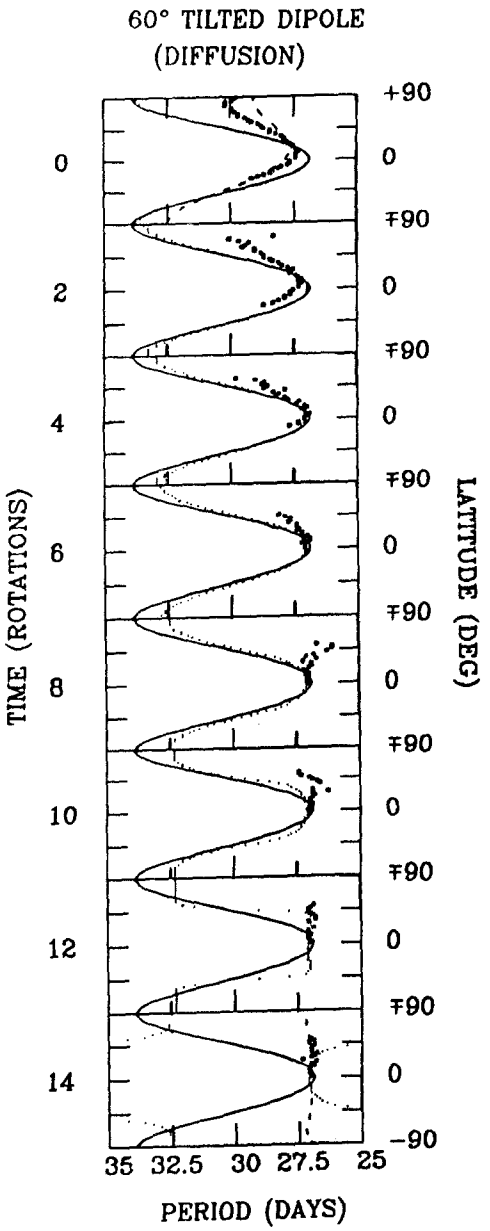

Fig. 6b. Rotation profiles for the yellow coronal hole of Figure 6(a) are indicated by the large dots. Also shown are the Newton–Nunn curve (solid lines), the projected source-surface rotation profiles (dashed lines in the first and last frames), and the rotation profiles of the polarity patterns of the photospheric field (dotted lines). After about 12 rotations, rigid rotation with a period of approximately 27 days is established from the equator to a latitude above 45°.

rotation profiles of Figure 7(b) show that the simulated hole rotates quasi-rigidly with a period near 27.5 days through most of its lifetime, as Timothy, Krieger, and Vaiana (1975) found for CH1.

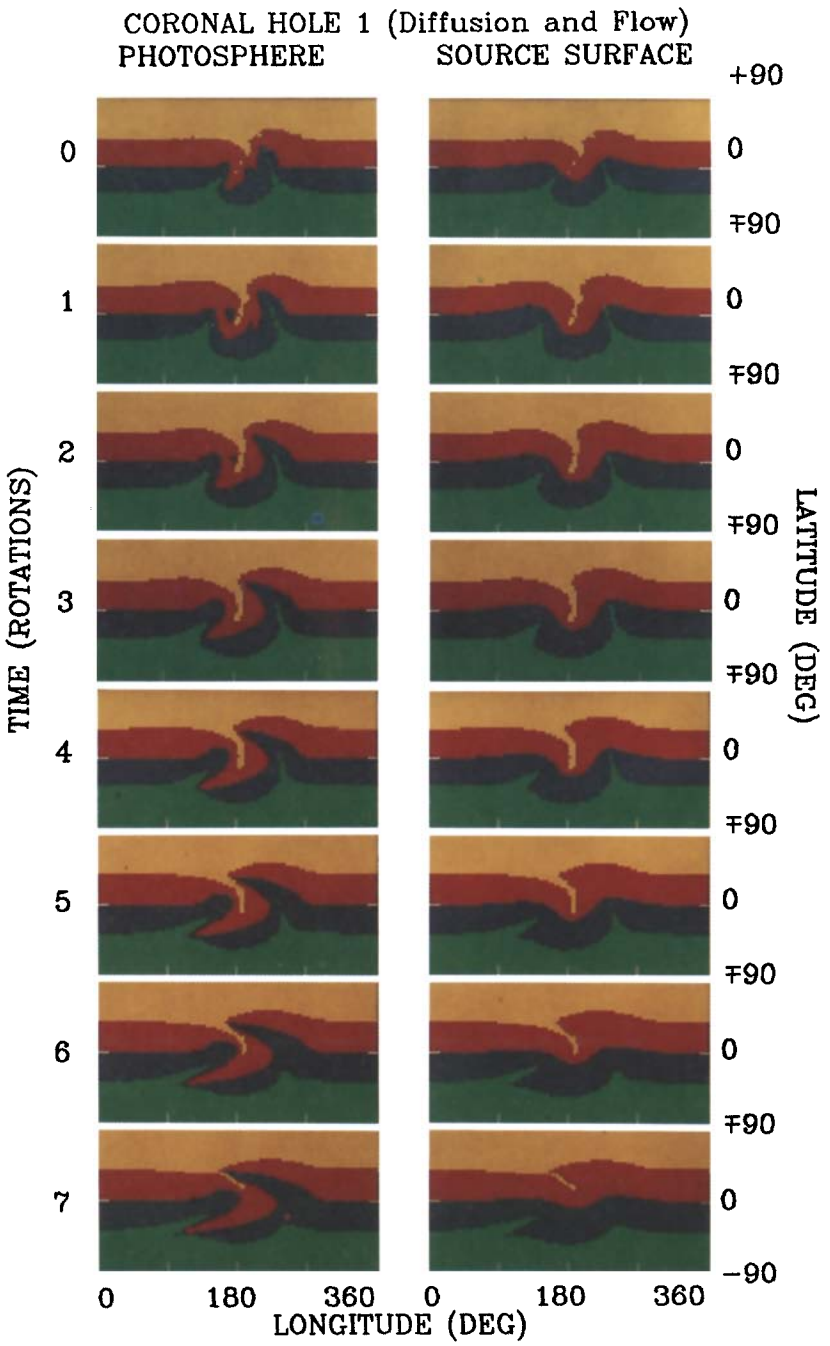

Fig. 7a. Evolution of an initial configuration similar to that of Skylab Coronal Hole 1 in May 1973. In this simulation, the initial photospheric flux distribution consisted of 5 doublet sources and a 1 G axisymmetric dipole field; flux transport was provided by differential rotation with the Snodgrass (1983) profile, supergranular diffusion at a 600 $km^2 s^{-1}$ rate, and a 10 $m s^{-1}$ latitude-independent poleward flow. For about 6 Carrington rotations, the yellow northern-hemisphere coronal hole maintains a relatively-undistorted meridional shape similar to that observed for CH1.

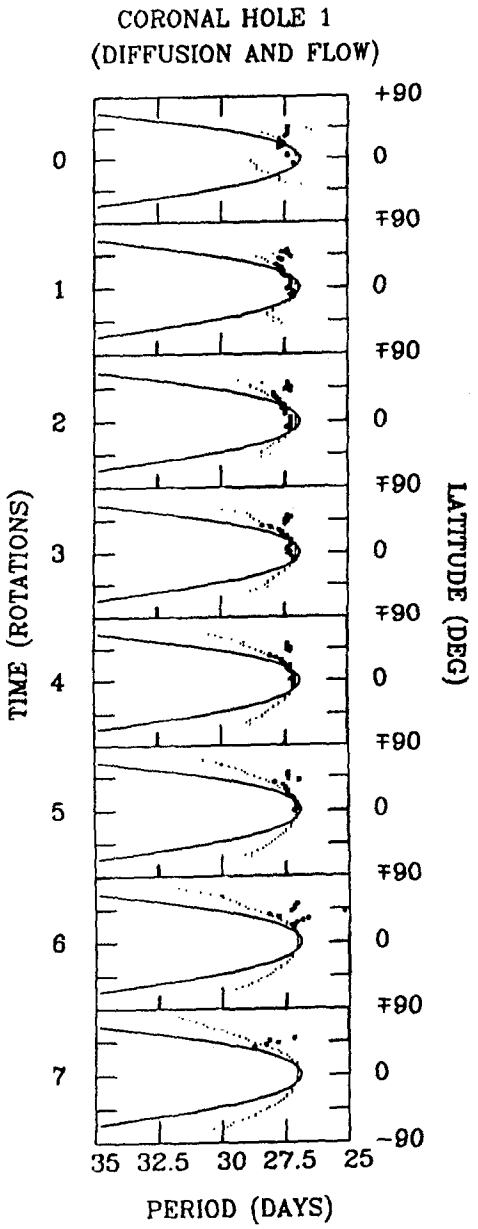

Fig. 7b. Rotation profiles for the yellow coronal hole in Figure 7(a), indicated by the large black dots. Also shown are the Snodgrass rotation curve (solid lines) and the rotation profiles of the polarity patterns of the photospheric field (dotted lines). Like Skylab CH1, the simulated hole rotates quasi-rigidly with a period of roughly 27.5 days throughout its 6–7 month lifetime.

In a related simulation which we do not display here, we found that the later evolution of the hole was not qualitatively changed by artificially turning off diffusion and flow after the hole became fully developed. Thus the rigid behavior of CH1 cannot be

attributed primarily to the presence of diffusion or flow. On the other hand, when we replaced the vertical-dipole field by an axisymmetric polar-field distribution ± 4.5 G $\cos^8\theta$ (which contains the same total flux), the coronal hole became appreciably more sheared than in Figure 8(a). (A $\cos^8\theta$ variation for the Sun's polar field during the period 1976–1977 was deduced empirically by Svalgaard, Duvall, and Scherrer, 1978.) This can be understood by noting that the greater poleward concentration of the $\cos^8\theta$ field shifts the neutral line to higher latitudes, and thus causes the opposite-polarity stripes to cut more rapidly into the polar-hole lobe. (Clearly, the hole would have been sheared less if the strength of the polar field had been increased to the value of 12 G advocated by Svalgaard, Duvall, and Scherrer, 1978.)

4. Summary and Discussion

In this study, we have seen that the rotation of a coronal hole is subject to both a coronal constraint and a photospheric one. On the one hand, the current-free condition requires the hole to follow its source-surface extension, which rotates quasi-rigidly. On the other hand, the hole must also remain within the confines of its photospheric polarity region, which in general rotates less rigidly than the source-surface field.

Within an unwound polarity pattern, a coronal hole is initially free to follow its coronal extension without violating the photospheric constraint. The actual rotation rate of the hole boundary depends on the phase velocities of all three field components at each intermediate height along the field lines, and thus only roughly matches the projected source-surface rate. Physically, it is the ongoing reconnection of magnetic field lines that uncouples the motion of the hole boundary from that of the underlying photospheric flux elements and allows the hole to follow the source-surface field.

The presence of a strong axisymmetric component of the field prolongs the unwound state of the photospheric field by forcing the neutral line to low latitudes where the shearing rate is small. This is normally the situation during the declining phase of the sunspot cycle, when the polar fields are strengthening and eruptions of non-axisymmetric flux are confined to zones close to the equator. We thus conclude that the dominance of the axisymmetric field component is responsible for the prolonged rigid rotation of large meridional coronal holes observed during that phase of the cycle (cf. Timothy, Krieger, and Vaiana, 1975). We emphasize that this rigid behavior does not require a systematic pattern of flux eruptions, as shown both by our simulations and by the empirical fact that Skylab CH1 continued to rotate rigidly in the absence of new sources.

When the axisymmetric component is weak and new sources are absent, we find that the photospheric polarity pattern becomes wound up into a series of azimuthally-oriented stripes, each with its own coronal hole. To satisfy both the coronal and photospheric constraints, the holes become coaligned in phase with the rigidly-rotating source-surface field, while simultaneously drifting equatorward within their confining photospheric polarity stripes. The hole boundaries themselves rotate instantaneously at the differential rate of the stripes.

Eventually, supergranular diffusion and meridional flow offset the shearing effect of

differential rotation (see Paper I). In particular, diffusion stops the formation of new stripes, while a poleward flow excludes them from an increasingly wide range of latitudes about the equator. These processes thus arrest the equatorward motion of the holes, which then rotate rigidly with the source-surface field. However, for the dipole configurations considered in this paper, more than a year was required for diffusion and flow to establish the rigid rotation, which exceeds the observed lifetimes of even the longest-lived coronal holes (Timothy, Krieger, and Vaiana, 1975; Sheeley and Harvey, 1981). Therefore, we would not expect these processes to contribute significantly to the rigid rotation of coronal holes near sunspot minimum, when the latitudinal gradients in the photospheric flux distribution are small and the rates of latitudinal flux transport are correspondingly slow. On the other hand, diffusion and (if present) meridional flow are largely responsible for the less rigid behavior of coronal holes near sunspot maximum, when the holes are constrained to rotate with the (partially-rigid) photospheric polarity stripes (cf. Paper I).

We have seen that magnetic field-line reconnection occurs whenever the boundary of a coronal hole rotates at a rate which differs from that of the local photospheric flux. This reconnection process was evident during the initial evolution of the horizontal-dipole configuration, when the large equatorial holes rotated with an initial 27.45-day equatorial period which exceeded the 26.9-day period of the photospheric flux, and was closer to the 27.68-day initial period of the source-surface field. The effect of reconnection was also apparent during the initial and later evolution of the axial holes of the tilted-dipole configuration, whose rotation at high latitudes was faster and more rigid than the local photospheric rate. These examples illustrate the point made in Paper II, that the rotation rate of the source-surface field is determined not by the footpoint latitudes of the open field lines, but by the latitudes where most of the unwound, non-axisymmetric flux is concentrated.

In Part C of the Appendix, we showed that the reconnection rate in the horizontal-dipole configuration is greatest during the first wind-up time, when the holes are largest and contain their maximum amount of flux. At an even earlier stage, one might also expect a large amount of reconnection to accompany the formation of new holes on the Sun, as strong bipolar magnetic regions emerge through the solar surface and interact with their surroundings. Such magnetic field-line rearrangements have been inferred from XUV images of the lower corona during the Skylab mission (Sheeley *et al.*, 1975a, b), and may lead to transient changes in coronal holes (Solodyna, Krieger, and Nolte, 1977; Webb *et al.*, 1978; Rust, 1983; Harvey and Sheeley, 1979; Harvey, Harvey and Sheeley, 1986).

On the other hand, our simulated coronal holes evolved toward final configurations – either dwindling remnants at the equator where the shearing rate approaches zero, or purely axisymmetric polar holes – where the reconnection rate asymptotically vanishes. Indeed, because the non-axisymmetric component of the source-surface field decays more rapidly than the axisymmetric component, any coronal hole containing a finite amount of axisymmetric flux will eventually end up as an axisymmetric polar hole. This accounts for the gradual disappearance of low-latitude holes and the dominance of polar

holes near sunspot minimum (cf. Waldmeier, 1951; Broussard *et al.*, 1978; Sheeley, 1980; Sheeley and Harvey, 1981).

Finally, we recall that the current-free model used in this paper is an idealized way of representing the structure of the coronal field. That large-scale currents are in fact present in the corona is suggested by the twisted fine structure of filaments and prominences. A more realistic model that allows for such localized currents would affect detailed aspects of our coronal-hole simulations, but would not alter our basic conclusions concerning the rotation of coronal holes. Indeed, not only is the evolution of the photospheric polarity patterns – and thus the photospheric constraint – unaffected by these currents, but the coronal field will continue to exhibit a quasi-rigid behavior so long as it remains dominated by low-order multipoles of the photospheric field (see Paper II). Comparisons with observed large-scale coronal structure and with MHD models such as that of Pneuman and Kopp (1971) have shown that potential-field calculations provide a reasonable first approximation to the coronal field inside the source surface (for references, see Hoeksema, 1984). We also note that the field-line reconnections suggested by Skylab images have been interpreted as evidence that the inner corona attempts to maintain a largely current-free state (Sheeley *et al.*, 1975a, b). Thus we would expect both the photospheric and coronal constraints on the rotation of coronal holes to remain applicable in a more refined treatment. Consequently, we would again find that a strong axisymmetric field component is responsible for the rigid rotation of the large meridional holes during the declining phase of the sunspot cycle, but that diffusion and flow determine the less-rigid rotation rates of the slanted holes seen near sunspot maximum.

Acknowledgements

We are grateful to our colleagues C. R. DeVore and R. A. Howard for a variety of helpful comments and advice. We also appreciate the computational assistance which L. R. Shampine (now at Lincoln Laboratory) provided in the early stages of this work. Financial support was provided in part by the Solar Physics Branch of the NASA Space Physics Division (DPR W-14429) and by the Office of Naval Research.

Appendix

Evolution of a Tilted-Dipole Configuration

In this Appendix, we derive some analytical results which facilitate the interpretation of the simulations of Section 3. We begin in Part A with a general formulation of the wind-up of a tilted-dipole configuration, and then study the initial and asymptotic behavior of the associated coronal holes in Parts B and C, respectively.

A. General formulation

We consider a tilted-dipole configuration which is subject to the differential rotation of the photosphere. The radial component of the photospheric field is then given by

$$B_{ph}(\theta, \phi, t) = \cos\xi \cos\theta + \sin\xi \sin\theta \sin[\phi - \omega(\theta)t], \tag{A1}$$

where ξ is the angle between the dipole axis and the Sun's north pole. We adopt a differential rotation profile of the form $\omega(\theta) = \omega_0 - \omega_1 \cos^2\theta$, where according to Newton and Nunn (1951) $\omega_0 = 13.39(\pi/180)$ rad day^{-1} and $\omega_1 = 2.77(\pi/180)$ rad day^{-1}, corresponding to an equatorial rotation period of 26.9 days and a wind-up time $\tau_w = 2\pi/\omega_1 = 130$ days.

Solving equations (A1) and (2) for the harmonic coefficients $a_{lm}(t)$ and substituting them into Equation (3), we obtain the components of the tilted-dipole field at an arbitrary radius $R_\odot \leq r \leq R_s$ and time t. In the coordinate system which rotates at the equatorial rate ω_0, these components may be written as:

$$B_r(r, \theta, \phi, t) = \sin\xi \sum_{l=1}^{\infty} N_{l1}^2 b_l(\alpha) c_l(r) P_l^1(\cos\theta) \sin[\phi + \beta_l(\alpha)] + \\ + c_1(r) \cos\xi \cos\theta, \tag{A2a}$$

$$B_\theta(r, \theta, \phi, t) = -\sin\xi \sum_{l=1}^{\infty} N_{l1}^2 b_l(\alpha) d_l(\alpha) \frac{\partial P_l^1(\cos\theta)}{\partial\theta} \sin[\phi + \beta_l(\alpha)] + \\ + d_1(r) \cos\xi \sin\theta, \tag{A2b}$$

$$B_\phi(r, \theta, \phi, t) = -\sin\xi \sum_{l=1}^{\infty} N_{l1}^2 b_l(\alpha) d_l(r) \frac{P_l^1(\cos\theta)}{\sin\theta} \cos[\phi + \beta_l(\alpha)]. \tag{A2c}$$

Here $\alpha = \omega_1 t$; $P_l^1(\cos\theta)$ are the associated Legendre functions whose normalization factors N_{l1} are given by $N_{l1}^2 = (2l + 1)/[2l(l + 1)]$ (Jahnke and Emde, 1945); the coefficients $c_l(r)$ and $d_l(r)$ are defined by Equations (4a) and (4b) of Section 2; and, finally, the amplitude $b_l(\alpha)$ and phase $\beta_l(\alpha)$ are determined by

$$b_l(\alpha)\, e^{i\beta_l(\alpha)} = \int_0^1 (1 - x^2)^{1/2} P_l^1(x)\, e^{i\alpha x^2}\, dx. \tag{A3}$$

We note that the integral in Equation (A3) vanishes unless l is odd, which means that only terms with odd l contribute to the sums in Equation (A2).

B. Initial Behavior

Our next step is to determine the initial behavior of the coronal-field components given by Equation (A2). For this purpose, we solve Equation (A3) for the harmonic amplitudes and phases in the limit $\alpha \ll 1$. As shown in Paper II, this can be accomplished by expanding $\exp(i\alpha x^2)$ in powers of α and retaining the first two non-vanishing integrals. Substituting the resulting expressions for b_l and β_l into Equation (A2) and retaining first-order terms, we obtain the desired field components

$$B_r(r, \theta, \phi, t) = c_1(r) \sin\xi \sin\theta \sin(\phi - \omega_r t) + c_1(r) \cos\xi \cos\theta, \tag{A4a}$$

$$B_\theta(r, \theta, \phi, t) = -d_1(r) \sin\xi \cos\theta \sin(\phi - \omega_\theta t) + d_1(r) \cos\xi \sin\theta, \tag{A4b}$$

$$B_\phi(r, \theta, \phi, t) = -d_1(r) \sin\xi \cos(\phi - \omega_\phi t), \tag{A4c}$$

where the respective phase velocities are given by

$$\omega_r(r, \theta) = \left\{\omega_0 - \frac{\omega_1}{5}\left[1 - \frac{c_3(r)}{c_1(r)}\right]\right\} - \omega_1\left[\frac{c_3(r)}{c_1(r)}\right]\cos^2\theta, \tag{A5a}$$

$$\omega_\theta(r, \theta) = \left\{\omega_0 - \frac{\omega_1}{5}\left[1 - 11\,\frac{d_3(r)}{d_1(r)}\right]\right\} - \omega_1\left[3\,\frac{d_3(r)}{d_1(r)}\right]\cos^2\theta, \tag{A5b}$$

$$\omega_\phi(r, \theta) = \left\{\omega_0 - \frac{\omega_1}{5}\left[1 - \frac{d_3(r)}{d_1(r)}\right]\right\} - \omega_1\left[\frac{d_3(r)}{d_1(r)}\right]\cos^2\theta. \tag{A5c}$$

From Equations (A4) and (A5), we see that each component of the magnetic field begins to rotate with its own distinct phase velocity which varies with radial distance from the Sun. The phase velocity of the radial component is already familiar to us from Paper II. At $r = R_\odot$ it reduces to the photospheric differential rate $\omega(\theta)$, whereas at $r = R_s$ it reduces to the quasi-rigid rotation rate of the source-surface field. The phase velocities of the non-radial components depend on the ratio d_3/d_1, which is smaller than c_3/c_1 (except at $r = R_s$ where the field is radial). Consequently, ω_ϕ is even more rigid than ω_r, but ω_θ may be less rigid, depending on the value of $R_s/R_\odot$.

Also, we note from Equation (A4a) that the radial field at arbitrary r initially satisfies the flux-transport equation (1), provided the photospheric angular rotation $\omega(\theta)$ is replaced by the radial phase velocity $\omega_r(r, \theta)$. This implies that the amount of flux which crosses the source surface does not change to first order in the elapsed time, but is simply redistributed by the effective source-surface differential rotation $\omega_r(R_s, \theta)$. Because this open flux originates within the photospheric coronal holes, such holes must contain a constant amount of flux as they begin to evolve.

Even though the total amount of flux within the coronal-hole boundary is initially conserved, this does not mean that the boundary deforms according to the motion of the photospheric flux elements located along it. The hole boundary suffers less distortion because its evolution is determined not just by $\omega(\theta)$, but by the relatively-rigid phase velocities $\omega_r(r, \theta)$, $\omega_\theta(r, \theta)$, and $\omega_\phi(r, \theta)$ at all radial distances along the open field lines. In fact, the process of tracking the photospheric footpoints of the source-surface neutral-line (and thus determining the coronal-hole boundary) is equivalent to computing weighted averages over the range $R_\odot \le r \le R_s$ of the three phase velocities given by Equation (A5). (The analytical expression for the initial coronal-hole rotation rate $\omega_{CH}(\theta)$ in terms of ω_r, ω_θ, and ω_ϕ is complicated and will not be reproduced here.) The behavior of the coronal-hole boundary contrasts with that of both the photospheric flux distribution and the source-surface field, whose rotation rates depend only on the phase velocities of the radial field at $R_\odot$ and R_s, respectively.

It is instructive to compare the actual coronal-hole rotation profile, $\omega_{CH}(\theta)$, with the source-surface rate as projected onto the photosphere along the open field lines. To derive the latter profile, we evaluate Equation (A5a) at $r = R_s$ and $\theta = \theta_s$, and transform

to the footpoint colatitude θ_F according to $\cos\theta_s = (\cos\theta_F - \cos\theta_c \cos\xi)/\sin\theta_c$, where θ_c represents the angular half-width of the coronal hole. Thus, expressed as a function of θ_F (which by definition must lie within the colatitudinal range of the hole), the source-surface rotation rate becomes

$$\omega_r(R_s, \theta_F) = \left\{\omega_0 - \frac{\omega_1}{5}\left[1 - \frac{c_3(R_s)}{c_1(R_s)}\right]\right\} - \\ - \omega_1\left[\frac{c_3(R_s)}{c_1(R_s)}\right]\left(\frac{\cos\theta_F - \cos\theta_c\cos\xi}{\sin\theta_c}\right)^2 . \tag{A6}$$

The profile (A6) is represented by the dashed curves in Figures 1(b) and 2(b) and 4(b), 5(b), and 6(b). These figures show that the projected source-surface rate provides only a crude zeroth-order approximation to the initial coronal-hole rotation rate. For the horizontal-dipole configuration, the agreement is best at the equator, where the coronal-hole period is 27.45 days as compared with 27.68 days for the corresponding source-surface period. However, the match becomes much poorer at latitudes above $\sim 30°$.

Finally, we derive a useful formula for the angular size θ_c of the initial pair of coronal holes, which are circles centered about the dipole axis. The heliocentric half-angle θ_c of each polar hole must be independent of the tilt angle ξ, which we therefore temporarily set equal to zero for simplicity. Recognizing that all of the flux which crosses the source surface must originate within the photospheric boundaries of these holes, we write

$$\int_0^{\pi/2}\int_0^{2\pi} B_r(R_s, \theta, \phi, 0) R_s^2 \sin\theta \,\mathrm{d}\theta \,\mathrm{d}\phi = \\ = \int_0^{\theta_c}\int_0^{2\pi} B_r(R_\odot, \theta, \phi, 0) R_\odot^2 \sin\theta \,\mathrm{d}\theta \,\mathrm{d}\phi . \tag{A7}$$

The radial fields at the photosphere, $c_1(R_\odot)\cos\theta$, and at the source-surface, $c_1(R_s)\cos\theta$, are obtained by setting $\xi = 0$ in Equation (A4a). Substituting these expressions into Equation (A7), we then deduce that

$$\sin^2\theta_c = \left(\frac{R_s}{R_\odot}\right)^2 c_1(R_s) = \frac{3(R_\odot/R_s)}{2 + (R_\odot/R_s)^3} . \tag{A8}$$

Physically, the quantity $f \equiv \sin^2\theta_c$ may be interpreted as the fraction of photospheric flux that reaches the source surface and thereby becomes open. For the nominal source-surface radius $R_s/R_\odot = 2.0$ used in our simulations, 70% of the flux is open and $\theta_c = 57.2°$. In the limit $R_s/R_\odot \to 1$, $f \to 1$ and $\theta_c \to \pi/2$, so that each coronal hole fills an entire hemisphere. In the opposite limit $R_s/R_\odot \to \infty$, $f \to 0$ and $\theta_c \to 0$, and the holes become vanishingly small.

It is interesting to note that the 57.2° half-angle is considerably larger than the 30° half-angle typically observed for polar coronal holes near sunspot minimum (Waldmeier,

1951; Bohlin, 1977; Sheeley, 1980). Indeed, Equation (A8) requires that the source surface be located at an unreasonably large distance of $R_s/R_\odot = 6$ in order to obtain a half-angle of 30°. This discrepancy can be resolved by considering a photospheric flux distribution of the form $B_{ph} = [(n+1)/2] \cos^n \theta$, which is more sharply peaked at the poles than a dipole field. Using Equation (A7), we find that for $n = 9$ this distribution gives $\theta_c = 35.0°$ if $R_s/R_\odot = 2.0$ and $\theta_c = 29.0°$ if $R_s/R_\odot = 2.5$. Such a sharply-peaked field is consistent with the one derived by Svalgaard, Duvall, and Scherrer (1978) from observations at the Wilcox Solar Observatory, and lends further support for the hypothesis that a poleward meridional flow may be present on the Sun (DeVore, Sheeley, and Boris, 1984).

C. Asymptotic behavior

Here, our objective is to determine the coronal-hole rotation rate for the tilted-dipole configuration after an elapsed time $t \gg \tau_w$. For this purpose, we return to Equation (A3) and evaluate the harmonic amplitudes and phases in the limit $\alpha \gg 2\pi$. As discussed previously by Sheeley and DeVore (1986) and in Paper II, the asymptotic behavior of this integral can be determined by expanding the integrand about $x = 0$ and $x = 1$. We then find that

$$b_l(\alpha)\, e^{i\beta_l(\alpha)} = P_l^1(0) \left(\frac{\pi}{\alpha}\right)^{1/2} e^{i\pi/4} + \frac{l(l+1)}{2} \frac{e^{i\pi} e^{i\alpha}}{\alpha^2}\,, \tag{A9}$$

provided that $\alpha \gg l(l+1)/4$. The two terms on the right-hand side of Equation (A9) represent the equatorial and polar asymptotes, respectively. Clearly, whenever this equation is valid, the equatorial asymptote dominates and gives

$$b_l(t) \sim t^{-1/2}\,; \qquad \beta_l = \pi/4\,. \tag{A10}$$

The condition $\alpha \gg l(l+1)/4$ can be expressed in terms of a 'critical' mode number l_c defined by

$$l_c = [8\pi(t/\tau_w)]^{1/2}\,. \tag{A11}$$

Now, at a given time, modes with $l \ll l_c$ will have attained their equatorial asymptotes, whereas modes with $l \gg l_c$ will not. As time proceeds, l_c will increase, and additional modes will reach their equatorial asymptotes. Nevertheless, there will always be still higher-order modes which have not yet become asymptotic and which, therefore, prevent the field as a whole from attaining its asymptotic state.

On the other hand, the field will become asymptotic if it depends on only a limited number of harmonic components. As we have discussed in Papers I and II, such a limitation occurs in the outer corona where the coefficients $c_l(r)$ and $d_l(r)$ decrease rapidly with increasing l. In this case, all of the contributing modes will eventually reach their equatorial asymptotes given by Equation (A10), which we can then substitute into

Equation (A2) to obtain

$$B_r(r, \theta, \phi, t) = \left(\frac{\pi}{\alpha}\right)^{1/2} \sin\xi \sin\left(\phi + \frac{\pi}{4}\right) \sum_{l=1}^{\infty} N_{l1}^2 P_l^1(0) c_l(r) P_l^1(\cos\theta) + \\ + c_1(r) \cos\xi \cos\theta, \tag{A12a}$$

$$B_\theta(r, \theta, \phi, t) = -\left(\frac{\pi}{\alpha}\right)^{1/2} \sin\xi \sin\left(\phi + \frac{\pi}{4}\right) \sum_{l=1}^{\infty} N_{l1}^2 P_l^1(0) d_l(r) \frac{\partial P_l^1(\cos\theta)}{\partial\theta} + \\ + d_1(r) \cos\xi \sin\theta, \tag{A12b}$$

$$B_\phi(r, \theta, \phi, t) = -\left(\frac{\pi}{\alpha}\right)^{1/2} \sin\xi \sin\left(\phi + \frac{\pi}{4}\right) \sum_{l=1}^{\infty} N_{l1}^2 P_l^1(0) d_l(r) \frac{P_l^1(\cos\theta)}{\sin\theta}. \tag{A12c}$$

Referring to Equations (A12), we see that the non-axisymmetric field components become oriented $\pi/4$ rad east of their initial longitude and decay slowly as $t^{-1/2}$; eventually, the axisymmetric component dominates the field. Thus, if Equations (A12) were valid all the way down to the photosphere, they would require that the coronal holes rotate rigidly at the equatorial rate. However, as $r \to R_\odot$, the coefficients $c_l(r)$ and $d_l(r)$ no longer decrease rapidly enough with l to limit the number of modes. Consequently, Equations (A12) become invalid, and the coronal holes never attain an asymptotic state of rigid rotation. In Section 3, we have witnessed this never-ending formation of stripes when differential rotation alone was included in our simulations.

If supergranular diffusion characterized by a global time-scale $\tau_d = R_\odot^2/\kappa$ were included in the flux-transport equation, it would introduce a mode-dependent decay factor $\exp[-l(l+1)t/\tau_d]$, and eventually limit the number of modes that contribute to the photospheric field (Leighton, 1964). As we found previously for the windup of a horizontal-dipole field, a nominal 300 km^2 s^{-1} diffusion would effectively prevent the formation of new modes after about 3.5 wind-up times and give rise to a two-zone rigid rotation at rates which differ only slightly from the equatorial and polar rates (Paper I; DeVore, 1987). Although we have not attempted to modify Equations (A12) to include diffusion, we have seen an example of the resulting asymptotic behavior in the numerical simulation of Figure 2.

Finally, because Equations (A12) are valid at the source surface, we can use them to evaluate the amount of open flux as a function of time. For simplicity, we consider only the horizontal dipole for which $\xi = \pi/2$. In this case, we can integrate Equation (A12a) to obtain the amount of positive flux $\Phi(t)$ which asymptotically threads the source surface. Expressing the result in terms of the amount of positive flux initially present, $\Phi(0) = \pi R_s^2 c_1(R_s)$, we find

$$\frac{\Phi(t)}{\Phi(0)} = \left(\frac{\pi}{\alpha}\right)^{1/2} \sum_{l=1}^{\infty} \frac{2l+1}{[l(l+1)]^2} \frac{c_l(R_s)}{c_1(R_s)} [P_l^1(0)]^3, \tag{A13}$$

where the sum is a slowly varying function of R_s. Evaluating it for $R_s/R_\odot = 2.0$ and using the relation $\alpha = \omega_1 t$, we finally obtain

$$\frac{\Phi(t)}{\Phi(0)} \simeq \frac{0.50}{(t/\tau_w)^{1/2}} \,. \tag{A14}$$

Thus, the open flux has virtually the same asymptotic time dependence as the amplitude of the dipole component and of the mean line-of-sight component of the field (Sheeley, 1981; Sheeley and DeVore, 1986). Again like these other field quantities, the amount of open flux does not change initially, but falls to about 50% of its initial value during the first windup time. This decrease of open flux must be compensated by an equal increase of closed flux because differential rotation alone cannot change the total amount of flux on the Sun. Clearly, the oppositely-directed magnetic field lines must reconnect as they encounter one another at the source-surface neutral line.

References

Altschuler, M. D. and Newkirk, G.: 1969, *Solar Phys.* **9**, 131.

Axford, W. I.: 1977, in M. A. Shea, D. F. Smart, and S. T. Wu (eds.), *Study of Traveling Interplanetary Phenomena*, D. Reidel Publ. Co., Dordrecht, Holland, p. 145.

Bohlin, J. D.: 1977, *Solar Phys.* **51**, 377.

Bohlin, J. D. and Sheeley, N. R., Jr.: 1978, *Solar Phys.* **56**, 125.

Broussard, R. M., Sheeley, N. R., Jr., Tousey, R., and Underwood, J. H.: 1978, *Solar Phys.* **56**, 161.

Bumba, V. and Howard, R.: 1965, *Astrophys. J.* **141**, 1502.

Chapman, G. A. and Sheeley, N. R., Jr.: 1968, in K. O. Kiepenheuer (ed.), 'Structure and Development of Solar Active Regions', *IAU Symp.* **35**, 161.

DeVore, C. R.: 1987, *Solar Phys.* **112**, 17.

DeVore, C. R. and Sheeley, N. R., Jr.: 1987, *Solar Phys.* **108**, 47.

DeVore, C. R., Sheeley, N. R., Jr., and Boris, J. P.: 1984, *Solar Phys.* **92**, 1.

Duvall, T. R., Jr.: 1979, *Solar Phys.* **63**, 3.

Fisher, R. and Sime, D. G.: 1984, *Astrophys. J.* **287**, 959.

Gabriel, A. H.: 1976, *Phil. Trans. Roy. Soc.* **A281**, 339.

Giovanelli, R. G.: 1980, *Solar Phys.* **68**, 49.

Hansen, R. T., Hansen, S. F., and Loomis, H. G.: 1969, *Solar Phys.* **10**, 135.

Harvey, J. W. and Sheeley, N. R., Jr.: 1979, *Space Sci. Rev.* **23**, 139.

Harvey, J. W. and Sheeley, N. R., Jr.: 1987, *Bull. Am. Astron. Soc.* **19**, 935.

Harvey, K. L., Harvey, J. W., and Sheeley, N. R., Jr.: 1986, in P. A. Simon, G. Heckman, and M. A. Shea (eds.), *Solar-Terrestrial Predictions: Proceedings of a Workshop at Meudon, France, June 18–22, 1984*, NOAA/AFGL, p. 198.

Hoeksema, J. T.: 1984, Ph.D. Thesis, Stanford University.

Hoeksema, J. T. and Scherrer, P. H.: 1987, *Astrophys. J.* **318**, 428.

Howard, R. and LaBonte, B. J.: 1981, *Solar Phys.* **74**, 131.

Jahnke, E. and Emde, F.: 1945, *Tables of Functions*, Dover, New York, p. 110.

Jones, H. P.: 1985, *Australian J. Phys.* **38**, 919.

Leighton, R. B.: 1964, *Astrophys. J.* **140**, 1547.

Levine, R. H., Altschuler, M. D., Harvey, J. W., and Jackson, B. V.: 1977, *Solar Phys.* **25**, 636.

McIntosh, P. S., Krieger, A. S., Nolte, J. T., and Vaiana, G.: 1976, *Solar Phys.* **49**, 57.

Newton, H. W. and Nunn, M. L.: 1951, *Monthly Notices Roy. Astron. Soc.* **111**, 413.

Parker, G. D.: 1986, *Solar Phys.* **104**, 333.

Parker, G. D., Hansen, R. T., and Hansen, S. F.: 1982, *Solar Phys.* **80**, 185.

Pneuman, G. W. and Kopp, R. A.: 1971, *Solar Phys.* **18**, 258.

Pneuman, G. W., Hansen, S. F., and Hansen, R. T.: 1978, *Solar Phys.* **59**, 313.

Pope, T. and Mosher, J.: 1975, *Solar Phys.* **44**, 3.
Rust, D. M.: 1983, *Space Sci. Rev.* **48**, 381.
Schatten, K. H., Wilcox, J. M., and Ness, N. F.: 1969, *Solar Phys.* **6**, 442.
Schatten, K. H., Leighton, R. B., Howard, R., and Wilcox, J. M.: 1972, *Solar Phys.* **26**, 283.
Sheeley, N. R., Jr.: 1980, *Solar Phys.* **65**, 229.
Sheeley, N. R., Jr.: 1981, *Astrophys. J.* **243**, 1040.
Sheeley, N. R., Jr. and DeVore, C. R.: 1986, *Solar Phys.* **103**, 203.
Sheeley, N. R., Jr. and Harvey, J. W.: 1978, *Solar Phys.* **59**, 159.
Sheeley, N. R., Jr. and Harvey, J. W.: 1981, *Solar Phys.* **70**, 237.
Sheeley, N. R., Jr., DeVore, C. R., and Boris, J. P.: 1985, *Solar Phys.* **98**, 219.
Sheeley, N. R., Jr., Nash, A. G., and Wang, Y.-M.: 1987, *Astrophys. J.* **319**, 481 (Paper I).
Sheeley, N. R., Jr., Bohlin, J. D., Brueckner, G. E., Purcell, J. D., Scherrer, V. E., and Tousey, R.: 1975a, *Solar Phys.* **40**, 103.
Sheeley, N. R., Jr., Bohlin, J. D., Brueckner, G. E., Purcell, J. D., Scherrer, V. E., and Tousey, R.: 1975b, *Astrophys. J.* **196**, L129.
Shelke, R. N. and Pande, M. C.: 1985, *Solar Phys.* **95**, 193.
Snodgrass, H.: 1983, *Astrophys. J.* **270**, 288.
Solodyna, C. V., Krieger, A. S., and Nolte, J. T.: 1977, *Solar Phys.* **54**, 123.
Stenflo, J. O.: 1974, *Solar Phys.* **36**, 495.
Stenflo, J. O.: 1977, *Astr. Astrophys.* **61**, 797.
Svalgaard, L., Duvall, T. L., Jr., and Scherrer, P. H.: 1978, *Solar Phys.* **58**, 225.
Timothy, A. F., Krieger, A. S., and Vaiana, G. S.: 1975, *Solar Phys.* **42**, 135.
Veeder, G. J. and Zirin, H.: 1970, *Solar Phys.* **12**, 391.
Wagner, W. J.: 1975, *Astrophys. J.* **198**, L141.
Waldmeier, M.: 1951, *Die Sonnenkorona*, Birkhauser Verlag, Basel.
Wang, Y.-M., Sheeley, N. R., Jr., Nash, A. G., and Shampine, L. R.: 1988, *Astrophys. J.* **327**, 427 (Paper II).
Webb, D. F., McIntosh, P. S., Nolte, J. T., and Solodyna, C. V.: 1978, *Solar Phys.* **58**, 389.
Wilcox, J. M. and Howard, R.: 1970, *Solar Phys.* **13**, 251.
Wilcox, J. M., Schatten, K. H., Tanenbaum, A. S., and Howard, R.: 1970, *Solar Phys.* **14**, 255.
Wilson, R. M.: 1979, *Results of Coronal Hole Research: An Update*, NASA Technical Memorandum 78237, MSFC, Huntsville, Alabama.
Zirker, J. B.: 1977a, *Rev. Geophys. and Space Phys.* **15**, 257.
Zirker, J. B.: 1977b, *Coronal Holes and High Speed Wind Streams*, Colorado Assoc. Univ. Press.